JOURNAL OF MATERIALS SCIENCE 23 (1988) 2339–2347

Hydrogen induced cracking in cold worked AISI 4140 steel welds

Y. B. SUN, J. E. INDACOCHEA
Department of Civil Engineering, Mechanics and Metallurgy, University of Illinois at Chicago, P.O. Box 4348, Chicago, Illinois 60680, USA

The relative susceptibility to hydrogen induced cracking of cold deformed AISI 4140 steel welds was investigated. Controlled amounts of diffusible hydrogen were introduced into these weldments by utilizing the gas metal arc welding process with additions of hydrogen to the shielding gas. The crack behaviour was measured in terms of total crack length and distance from the fusion line. The crack propagated along the coarse grain structure of the HAZ about the fusion line. The refinement of the grain resulting from the increased cold roll reduces the crack activity. The susceptibility to hydrogen induced cracking of the cold worked samples appear to be sensitive to a critical value of residual stresses and to the orientation of the weld with respect to the rolling direction.

1. Introduction

Service failures due to fatigue and brittle fracture of welded structures may originate at small pre-existing cracks in the heat-affected zone (HAZ) near the fusion boundary. Some of the most common HAZ cracks are caused by the presence of hydrogen in the weld. Hydrogen sources can be raised by any hydric compounds intervening in the welding astmosphere, which are dissociated into atomic hydrogen at the very high temperature in the arc [1]. It has been claimed that a portion of the hydrogen dissolved in a molten weld pool may be transported to the solidified region by the hydrogen-saturated liquid metal due to the electromagnetic stirring action [2]. At the outer perimeters of the pool, as the solubility of gas decreases with temperature, the hydrogen internal solution pressure increases in the instantaneously solidified layer compared with the neighbours. This pressure provides the driving force for hydrogen to diffuse both into the solid metal and back into the molten pool [3]. It has been indicated that hydrogen is usually trapped at dislocations, grain boundaries, microinclusions, and structural heterogeneities [4]. This trapped hydrogen causes decohesion of grain boundaries and eventually nucleates microcracks in conjunction with the residual stresses [5–7].

Cold cracking, or hydrogen-induced cracking, is perhaps the most serious and least understood of all weld cracking problems. The various factors that influence hydrogen cracking are well documented [8]. Prior to crack initiation there is usually a time delay, and crack propagation occurs in a slow, jerky mode, with further incubation times between steps in the crack growth. Generally at crack initiation and at low crack growth rates, it has been found that cracking is intergranular and along prior austenite grain boundaries [9]. However, the crack can also be transgranular [10]. The initiation of cold cracking is particularly associated with notches or microstructural inhomogenieties which exhibit sudden changes in hardness, such as slag inclusions, martensite–ferrite interfaces and even grain boundaries.

The gradual loss of notch toughness of samples charged with hydrogen has been well characterized experimentally [11–14]. This effect has also been tested on ductile, spheroidized steel microstructures [11, 12], and it was observed that the losses in ductility were reflected by the changes in the dimple sizes on their fracture surfaces. The presence of non-metallic inclusions [12], however, has been found to influence the void growth rate in the ductile microstructure when charged with hydrogen.

Cold cracks have been observed in a wide range of microstructures. In the HAZ they are most commonly (but not necessarily) associated with martensitic structures. Prior to the austenite to martensite phase transformation, as the temperature drops there is a decrease in hydrogen solubility during the transformation, which corresponds to an increase in diffusivity. As the transformation proceeds the austenite becomes progressively more enriched in hydrogen. This has been thought to be a possible explanation of why cold cracking is so sensitive to the presence of martensite [1].

Studies of hydrogen in cold-worked steel have shown that both the solubility and the diffusion rate are significantly changed when the steel is cold worked. Darken and Smith [15] discovered that the amount of hydrogen absorbed from acid by cold-rolled steel at 35° C is many times greater than that absorbed by hot-rolled steel. Keeler and Davis [16] confirmed the high apparent solubility of hydrogen in cold-worked iron–carbon alloys at temperatures up to and even beyond the recrystallization temperature. Hill and Johnson [17] explained that the formation of microcracks by dislocation pileups is presumably the first

0022–2461/88 $03.00 + .12

step in the mechansim of fracture of their cold-rolled iron–carbon alloys.

A common view of hydrogen embrittlement of steel is that it is always plastically deformed to some extent. Such permanent deformation could exist in steel parts as a result of their fabrication process, particularly when submitted to some form of cold work. In this study, a hardenable steel (AISI 4140) submitted to different levels of cold work is welded by utilizing the gas metal arc welding (GMAW) process. Controlled amounts of diffusible hydrogen were introduced into these weldments by doping the shielding gas with different additions of Ar–2.5% H_2.

2. Materials and procedures

One heat of 0.625 in. (15.88 mm) AISI 4140 steel plate and one heat of AWS type ER70S-3 spooled filler metal wire were used in this study. The chemical compositions and mechanical properties of these materials are presented in Table I. The steel plates were normalized at 880° C for one hour and then machined to thicknesses such that after different levels of cold work (5, 10 and 20% primarily), the coupons would have a thickness of 0.5 in. (12.7 mm). Following cold work, specimens were cut perpendicular and parallel to the rolling direction to dimensions of 2.0″ × 0.5″ × 0.3″ (50.8 mm × 12.7 mm × 7.6 mm).

2.1. Welding and hydrogen content of weld metal

Welding was performed using gas–metal arc-welding (GMAW) by depositing a single bead on the small specimens. The samples were arranged in a fixture which included run-off tabs and spacers between them, as shown in Fig. 1, to facilitate separation of the weld specimens. The shielding gas, Ar–2.0% O_2, was doped with Ar–2.5% H_2 so as to produce four different levels of hydrogen, 2.5, 1.5, 1.0 and 0.25% adjusted from the flow rates. The shielding gas flow was maintained constant at 40 $ft^3 h^{-1}$ (1.132 $m^3 h^{-1}$). The welding parameters used were 24 V, 220 A and a travel speed of 15 in min^{-1} (381 mm min^{-1}). All material, including start-up and run-off tabs were degreased with acetone immediately prior to welding.

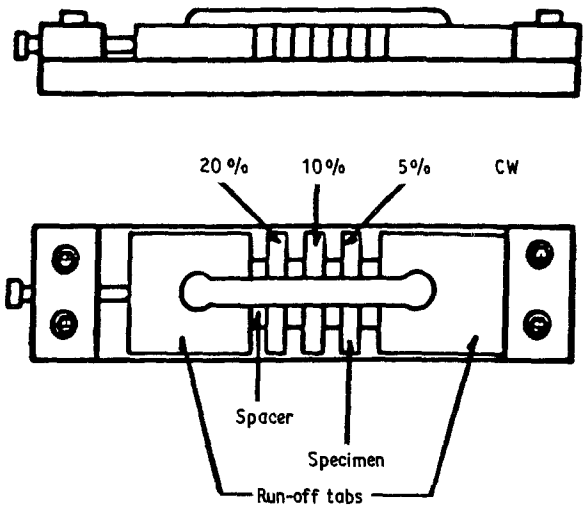

Figure 1 Welding fixture for holding the specimens during the welding process.

2.2. Treatment of weld specimens

Following welding, the weld specimens were removed from their fixture and water quenched within 5 sec. The samples were then transferred momentarily to a bath of dry ice and ethanol at −40° C and later stored in liquid nitrogen at −196° C.This procedure was used to prevent hydrogen loss. Each specimen was separated from the attached spacer without significant warming by using a slitting saw and the specimen immersed in a container filled with methanol and dry ice.

The saw-cut faces of the weld samples were repolished to facilitate microscopic observation of cracking during later testing. During repolishing, care was taken to avoid significant warming of the specimens and prevent hydrogen loss.

2.3. Augmented strain cracking test (ASCT) [18]

The same procedure established by Savage *et al.* [18] was attempted in this portion of the study. The specimens were loaded into the augmented strain cracking test fixture (Fig. 2) to produce consistent strains. The samples were forced to conform to the surface of the radius-die block by manually tightening the bolt.

TABLE I Chemical composition and mechanical properties of base and filler metals

Material	Composition (w/o)						
	C	Mn	P	S	Si	Cr	Mo
AISI-4140 Base-Plate	0.38–0.43	0.75–1.00	0.040 max	0.040 max	0.20–0.35	0.80–1.10	0.15–0.25
ER-70S-3 Filler Metal (0.45″ (1.14 mm) dia)	0.06–0.15	0.90–1.40	0.025 max	0.035 max	0.45–0.70	–	–
	Mechanical properties						
	Yield Strength (psi)	Tensile Strength (psi)	Elongation (%)		Reduction of area (%)		Hardness (BHN)
AISI-4140 Base Plate (Normalized)	95 000	148 000	17.7		46.8		302
ER-70S Filler Metal (0.045″ (1.14 mm) dia)	60 000	72 000	22.0		–		–

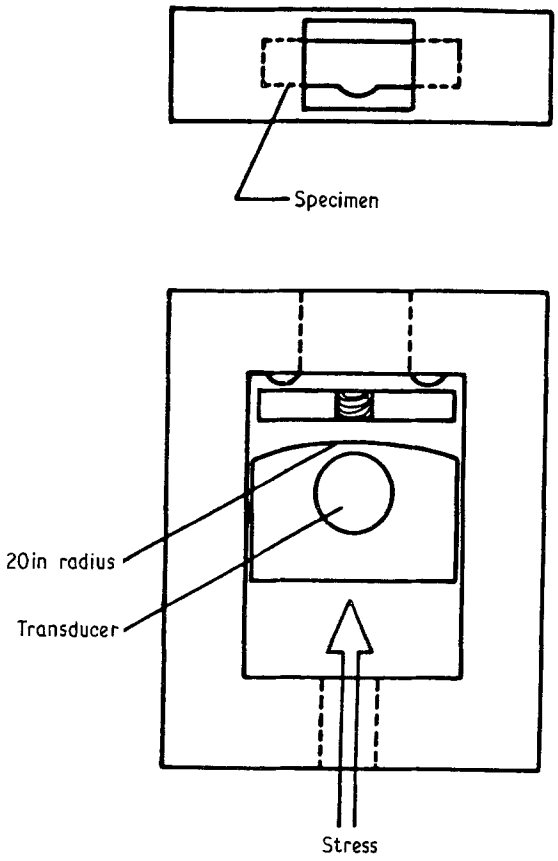

Figure 2 Fixture for the augmented-strain cracking test (ASCT).

However, it was difficult to control the strain rate and applied load consistently, a couple of weld samples produced with just Ar–2.0% O_2 shield gas had cracks unexpectedly.

After the samples were strained in the ASCT device for different times, they were inspected under the light microscope in order to follow the crack development. However, it was observed that further cracking would occur long after the samples had been removed from the strain fixture. Weld samples which were not subjected to ASCT also developed cracking when they were aged at room temperature after being stored in liquid nitrogen. Since no variable strains were introduced by just ageing the weld specimens this last procedure was followed to keep the strain conditions unchanged, and just subject to the residual stresses resulting from solidification, thermal cooling and phase transformations. A set of weld samples were processed with Ar–2% O_2 to check for possible quench cracks, but none could be observed.

2.4. Metallographic procedures and microhardness

Samples were examined under the light microscope in the as-polished condition to identify cracking. The crack susceptibility was estimated by measuring the total crack length and their average location with respect of the fusion line in the HAZ. The microstructure was revealed by etching the specimens with a 2% nital solution. Grain size measurements were performed according to ASTM standard E112. An etchant of saturated picric acid and sodium tridecylbenzene sulphonate was used to bring out the prior austenitic grain boundaries, as shown in Fig. 3.

Microhardness indentations were made in the HAZ at intervals of 0.2 mm starting at the fusion line toward the unaffected base metal. A load of 300 g was applied for 15 sec for each indentation.

3. Results and discussion

3.1. Metallographic studies

Since grain growth in the HAZ of alloy steels is reported to occur unrestricted at temperatures above

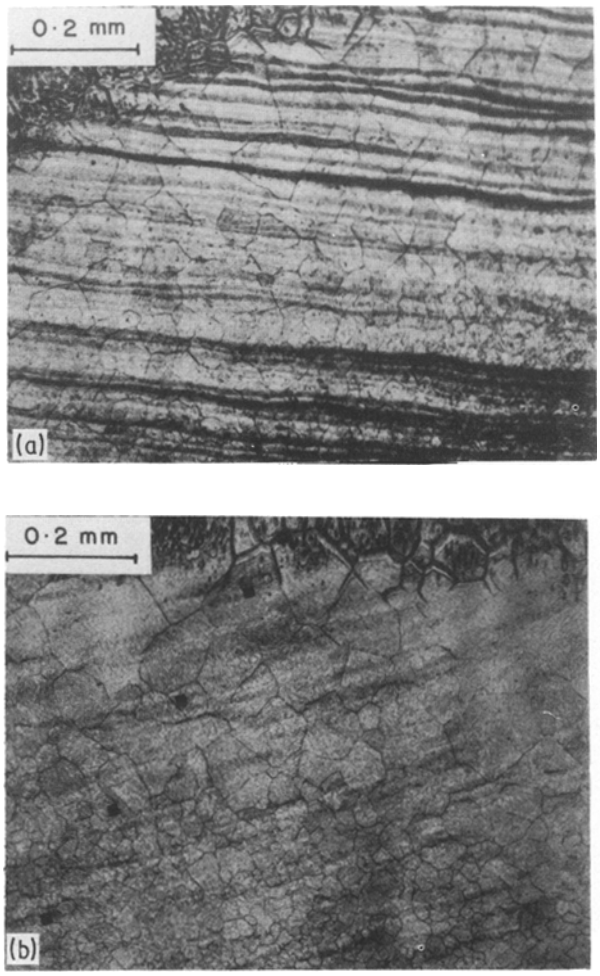

Figure 3 Photomicrograph depicting the prior austenite grain boundaries about the fusion line in the HAZ for three weld specimens. (a) 5% CW (b) 10% CW (c) 20% CW.

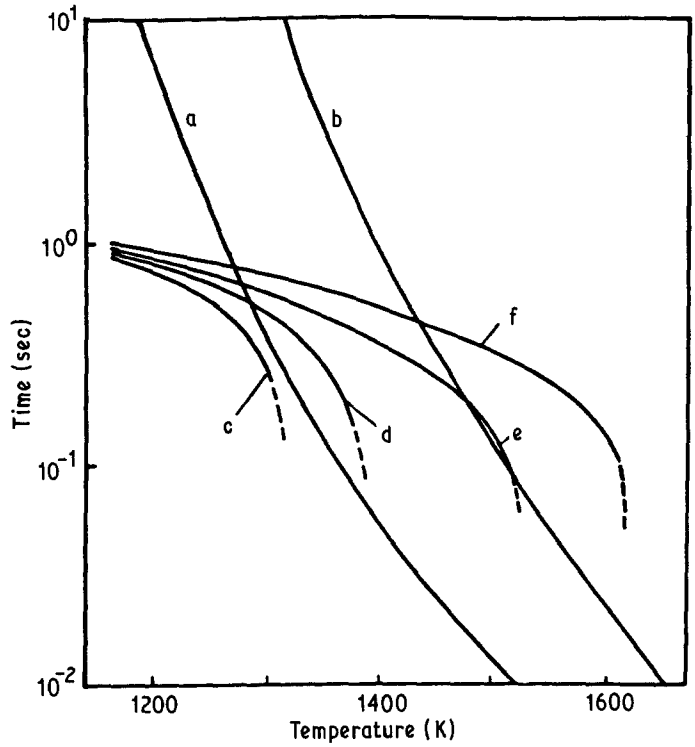

Figure 4 Diagram representing the carbide dissolution curves (a chromium, b molybdenum) with the estimated cooling curves for specific locations within the HAZ. (c 0.8 mm, d 0.6 mm, e 0.4 mm, f 0.2 mm).

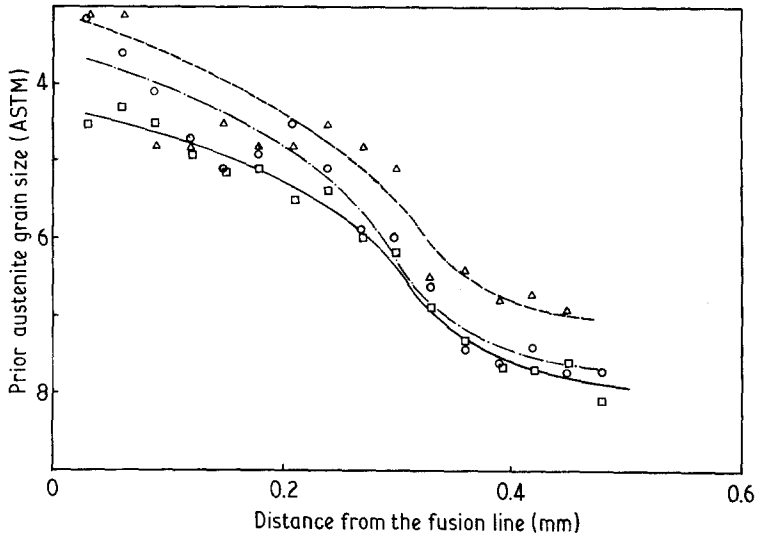

Figure 5 Grain size distribution as a function of amount of cold work and distance from the fusion line in the HAZ. All the weld samples were welded using a shielding gas with 0.25% H_2. (– – –△ 5% CW, –·–·–○ 10% CW, ——□ 20% CW).

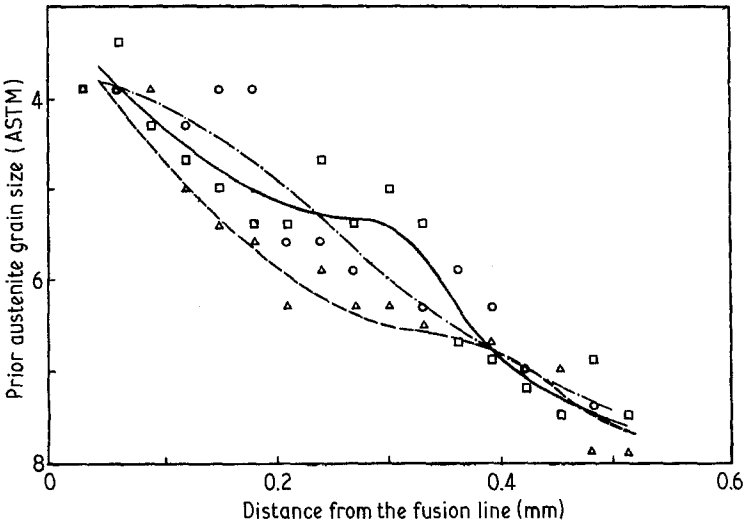

Figure 6 Grain size distribution as a function of amount of cold work and distance from the fusion line in the HAZ. Welds were produced with a shielding gas containing 2.5% H_2. (– – –△ 5% CW, –·–·–○ 10% CW, ——□ 20% CW).

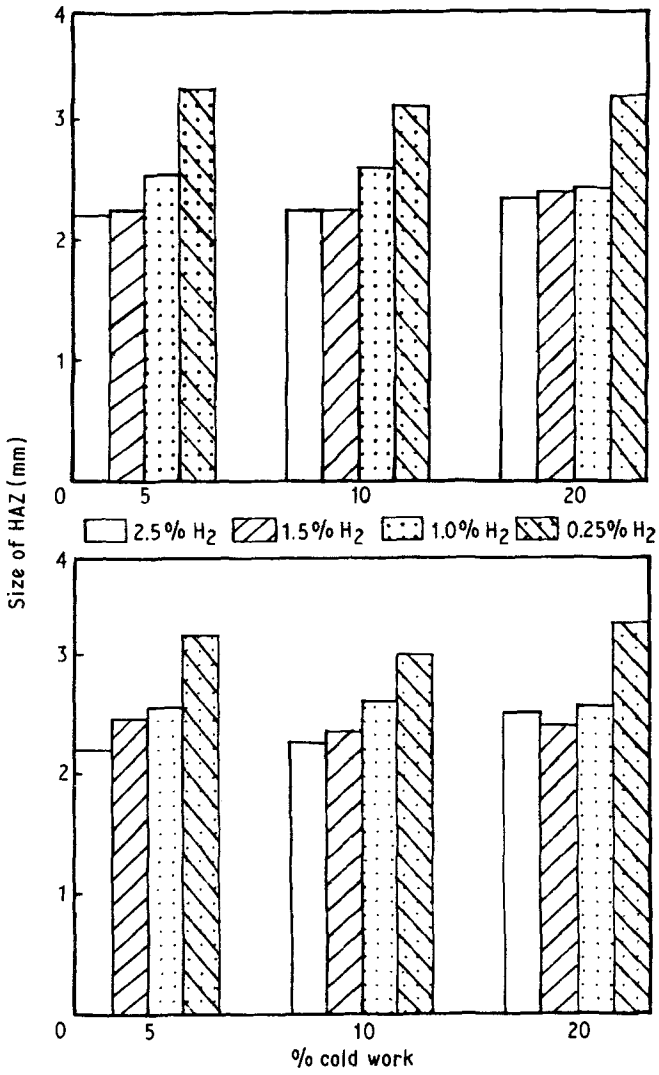

Figure 7 Width of the heat affected zone as a function of the hydrogen content in the shielding gas for different amounts of cold work. (a) longitudinal (b) transversal.

which the carbides are in solution [19], the extent of such region in the present study was estimated to define the range for the grain size measurements. In establishing this particular zone, the peak temperatures and the heating and cooling rates were measured via thermocouples inserted at intervals from the weld centre line in the HAZ. The information was used to estimate the time–temperature distributions for locations at 0.2, 0.4, 0.6 and 0.8 mm from the fusion line, by applying the Rosenthal empirical equations [20]. These curves have been superimposed on the carbide dissolution curves for chromium molybdenum, as shown in Fig. 4. Based on these results, it was established that the prior austenite grain size measurements should be conducted up to a distance of 0.6 mm from the fusion line.

It was observed that in the HAZ of weld samples produced with the shielding gas containg 0.25%

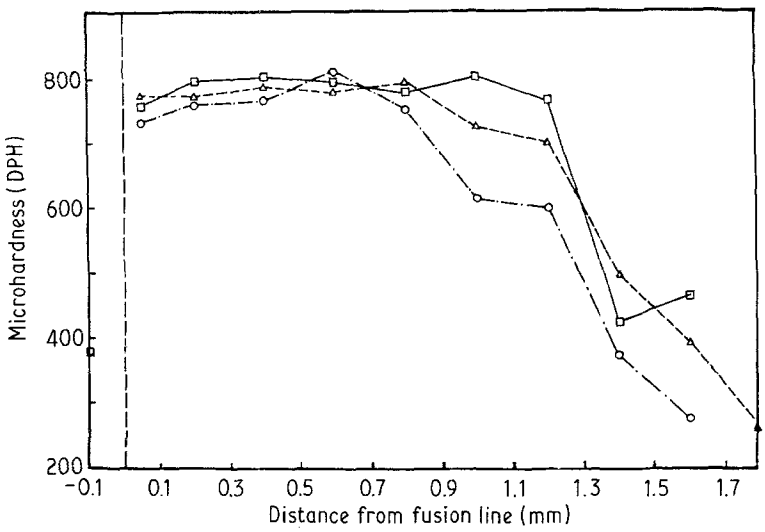

Figure 8 Microhardness variation in the HAZ for different amounts of cold work (△ 5%, ○ 10%, □ 20%) as a function of distance from the fusion line. Welds produced with a shielding gas containing 1.0% H_2.

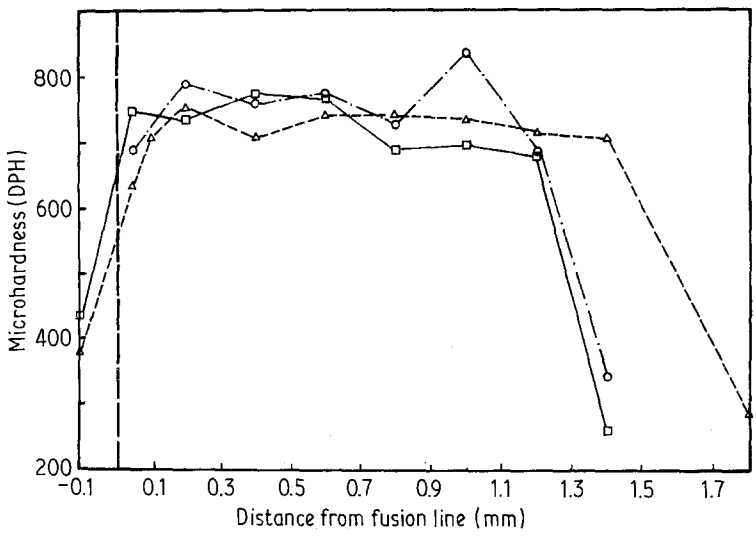

Figure 9 Microhardness variation for the 10% cold worked weld specimens and different shielding gases. (△ 0.25% H_2, ○ 1.5% H_2, □ 2.5% H_2).

hydrogen the grain structure became finer as the amount of cold work increased, as seen in Fig. 5. However, this did not occur in weld samples produced with 1.5 and 2.5% H_2 shielding gas, Fig. 6. Such discrepancy could be attributed to the welding arc stability; the arc became unstable as the level of hydrogen in the shielding gas was increased above 1.0%. This instability apparently lowers the heat input, which is manifested by the decrease in the width of the heat-affected zone when the amount of hydrogen in the shielding gas increased from 0.25% to 2.5% H_2, Fig. 7. In addition there was considerable spattering and porosity in the welds processed with the unstable arc.

The microhardness measurements within the region defined for the grain size measurements, were found to be relatively uniform for all the specimens. Such values ranged between 600 and 800 DPH within 1.0 mm from the fusion line, and then dropped to lower values reaching 300–400 DPH in the unaffected base metal. Some of these results are shown in Figs 8 and 9.

3.2. Crack behaviour

Hydrogen-assisted cracks were observed at or near the surface cross-section for most of the weld specimens and within the coarse grain region of the HAZ. These cracks were found to be primarily intergranular, but transgranular crack paths were also found along lath martensite boundaries (Figs 10 and 11), and most of these cracks propagated parallel to the fusion line, as seen in Fig. 12.

In evaluating the effect of cold work on hydrogen

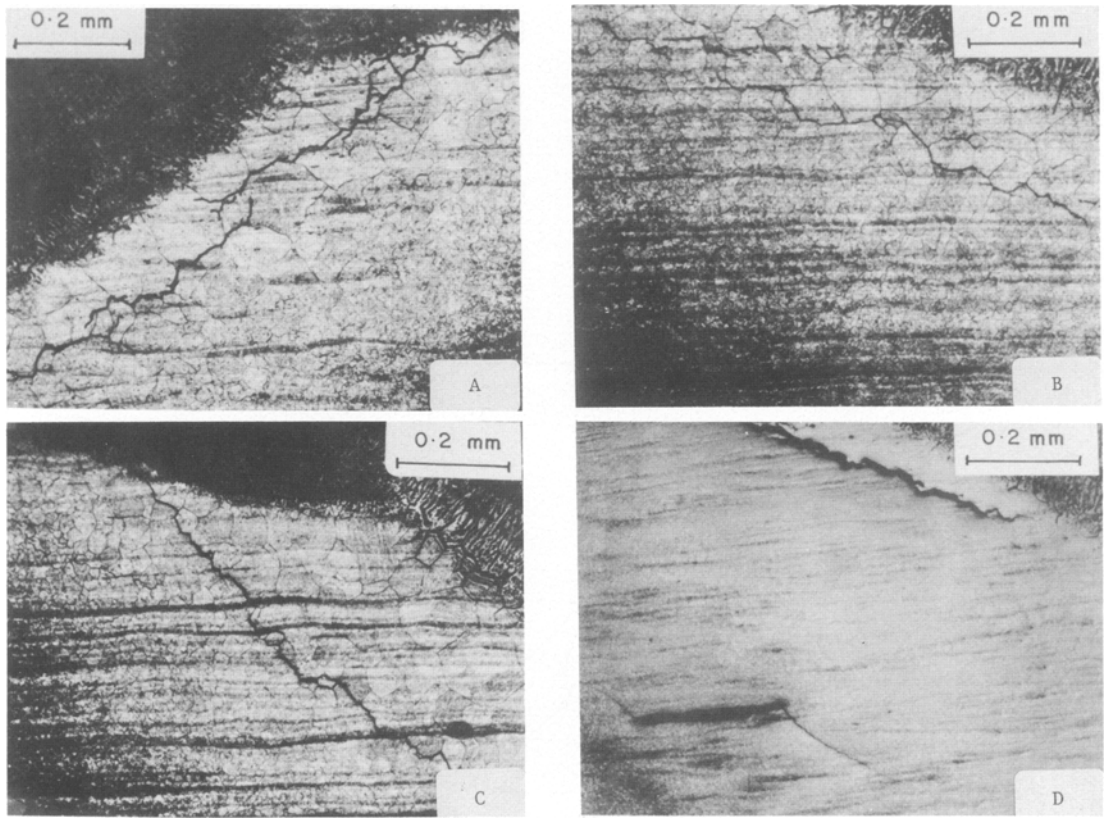

Figure 10 Crack patterns in the HAZ of weld specimens with different amounts of cold work: (a) 5%, (b) 10%, and (c) 20%. The micrograph in (d) shows an inclusion and small cracks resulting from it. All the welds used a 1.0% H_2O shield gas.

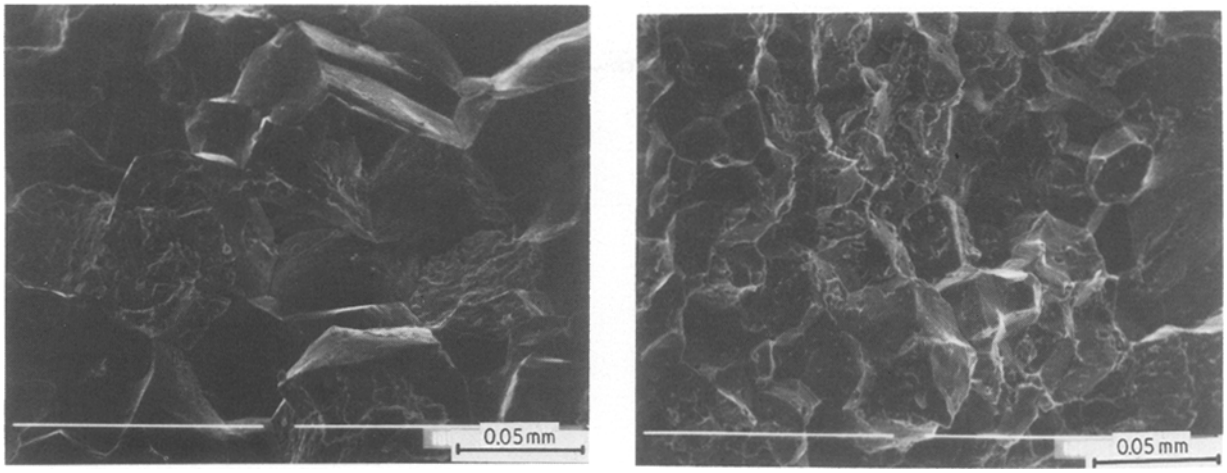

Figure 11 Fractographs depicting the intergranular cracking found in the HAZ of the weld specimens. Spots of transgranular cracking are also observed.

induced cracking, the lengths of all the HAZ cracks are summed to arrive at a quantitative measure of cracking susceptibility. The approximate average location of the cracks with respect to the fusion line was also measured. It was found that the orientation of the weld bead with respect to the rolling direction did influence the crack susceptibility, samples with the weld bead perpendicular to the rolling direction (transversal weld specimens) had larger total crack lengths than the longitudinal weld specimens for corresponding levels of cold work, as shown in Fig. 13. Such results would be expected due to the opposite action of the residual stresses resulting from both the rolling and welding processes as is the case of the transversal samples.

The hydrogen crack susceptibility in terms of the amount of cold work was examined only in the samples processed with shielding gases containing

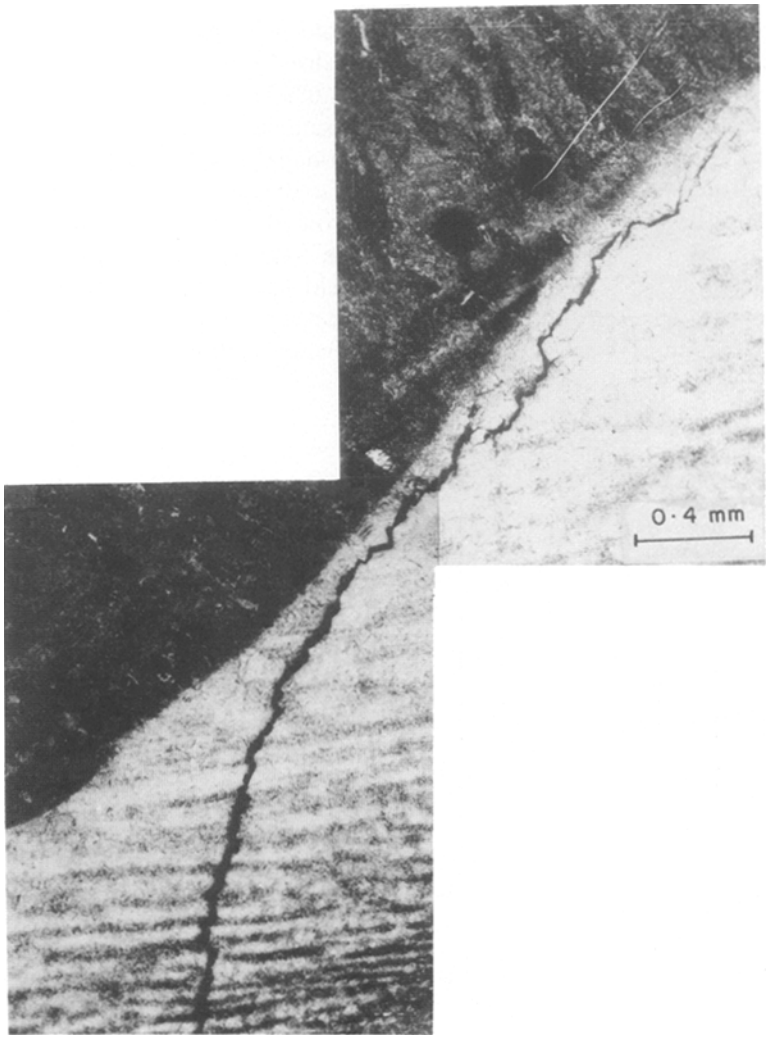

Figure 12 Micrograph showing the crack propagation parallel to the fusion line in the coarse grain region.

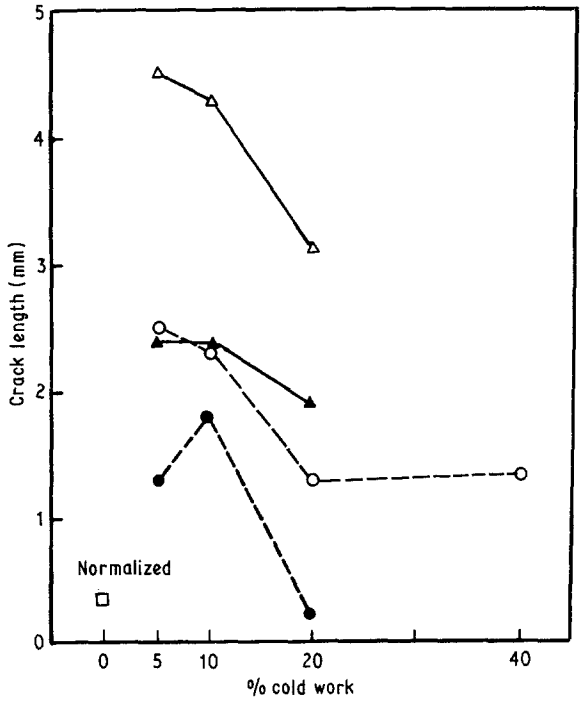

Figure 13 Average crack length as a function of cold work and sample orientation. (● ▲ 0.25% H_2, □ ○ △ 1.0% H_2, —— transversal, – – – longitudinal).

0.25 and 1.0% H_2, because only at these hydrogen levels the arc remained stable. As expected, the weld specimens produced with the 1.0% H_2 shielding gas had the longest crack lengths, as observed in Fig. 13, because higher hydrogen levels are anticipated in these samples compared to those produced with the 0.25% H_2 shield gas. In both cases it was found that the crack susceptibility decreased as the amount of cold work increased, especially beyond 10%. A possible explanation for such behaviour could be found in the structural changes occuring in the HAZ. It was observed that the samples that were cold reduced 5% had a coarser grain structure than the 10% and 20% cold worked specimens, as shown in Figs 5 and 14. The coarse grain structure increases the hardenability, because the decrease in the grain boundary area reduces the possible transformation of ferrite products. The decrease of the grain boundary will also reduce the high diffusivity paths causing the concentration of hydrogen per grain boundary area to increase, and thus resulting in higher pressures. This increase in pressure must be real, since larger crack lengths were observed in the 1.0% H_2 welds than in the 0.25% H_2 welds for equivalent amounts of cold work, as seen in Fig. 13. Note that the crack activity did not change for the one set of samples cold deformed 40%, which suggests that there must be a limiting degree of deformation for maximum improvement in hydrogen crack susceptibility among the deformed samples. Recall that only the grain size changed within this narrow region (0.6 mm from the fusion line); the martensitic microstructure and microhardness (Figs 8 and 9) stayed unchanged, regardless of the prior amount of cold work. The values measured for the microhardness far exceeded the critical value of 330 DPH to cause hydrogen cracking.

It was also observed that the average crack location from the fusion line increased as the amount of cold work was reduced, as shown in Fig. 15. Since the cracks occurred in the coarse grain region of the HAZ, this result would be expected because the average coarse grain size for the samples cold worked 20% is smaller than the 5% cold worked samples. The few samples cold worked 40% had the cracks even closer to the fusion line (Fig. 15) and also small longitudinal crack lengths (Fig. 13). As can be seen in Fig. 13, the crack activity of the cold deformed weld specimens was greater than normalized weld specimens, for the welds processed with 1.0% H_2 shield gas. The 20% and 40% cold worked samples revealed a finer grain structure than the normalized weld sample, which implies that in addition to the microstructure, remaining residual stresses from the cold work operation could play a role in the crack susceptibility. Among the same deformed weld specimens, a difference is found between the transversal and longitudinal weld samples, which raises the speculation that distribution

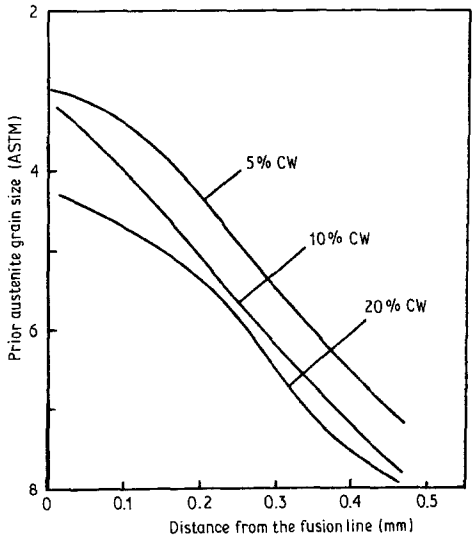

Figure 14 Grain size distribution as a function of percentage cold work and distance from the fusion line in the HAZ. All welds were produced with a shield gas containing 1.0% H_2.

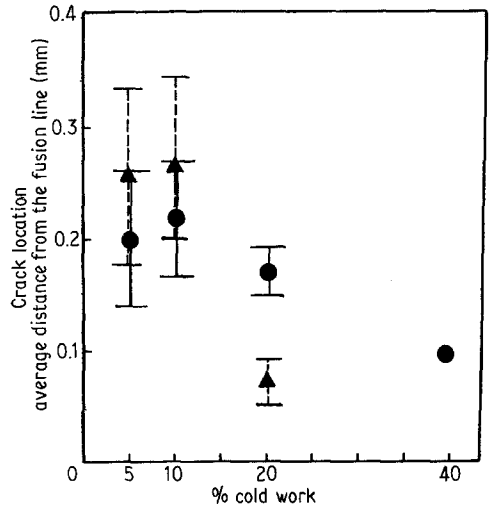

Figure 15 Average crack location in the HAZ as a function of cold work for welds produced with shielding gases containing 0.25 (▲) and 1.0% (●) H_2.

of residual stresses may impact on crack susceptibility. Similar results were found between the transversal and longitudinal specimens in the 0.25% H_2 shield gas welds. The hydrogen levels in the welds do influence the crack magnitude, as noted, and these levels were high in the present investigation. Further studies are currently underway using lower hydrogen levels and larger amounts of cold work to evaluate the effect of the remaining residual stresses.

4. Conclusions

The conclusions drawn from this investigation of the hydrogen induced cracking in cold worked AISI 4140 steel welds are

(1) Cold work can enhance the susceptibility of hydrogen induced cracking in high alloy steels.

(2) Grain refinement among the cold worked weld specimens apparently reduces the hydrogen crack susceptibility, but cannot overcome the negative effects of the residual stresses present.

(3) Weld specimens with the bead perpendicular to the rolling direction (transversal samples) are more susceptible to hydrogen cracking than the longitudinal samples. This suggests that the level and distribution of residual stresses affect hydrogen cracking.

References

1. F. R. COE, "Welding Steels without Hydrogen Cracking", (The Welding Institute Publication, Cambridge, 1973).
2. R. A. WOODS and D. R. MILNER, *Welding J.* **50** (1971) 163.
3. D. G. HOWDEN, *ibid* **61** (1982) 103.
4. C. V. KHALDEEV, "Formation and Development of Microcracks in Electric Sheet with Hydrogenation", Dep. VINITI, No. 3177-75 (1976).
5. C. F. BARTH and E. A. STEIGERWALD, *Met. Trans.* **1** (1970) 3451.
6. N. J. PETCH, *Phil. Mag.* **1** (1966) 331.
7. G. SUNDARARAJAN and P. G. SHEWMON, *Met. Trans.* **12A** (1981) 1761.
8. A. T. FIKKERS and T. MULLER *Welding in the World* **143** (1976) 238.
9. G. E. KERNS, M. T. WANG and R. W. STAEHLE, "Stress Corrosion Cracking and Hydrogen Embrittlement of Iron Base Alloys", NACE-5, p. 700, NACE, Houston, (1977).
10. S. K. BANERJI, C. J. McMAHON and H. C. FENG *Met. Trans.* **9A** (1978) 237.
11. R. GARBER, I. M. BERNSTEIN and A. W. THOMPSON, *Scripta Metall.* **10** (1976) 341.
12. I. E. FRENCH, P. F. WEINRICH and C. W. WEAVER, *ibid* **13** (1979) 285.
13. E. A. SAVCHENKOV and A. F. SVETLICHKIN, *Metallovedenie i Termicheskaya Obrabotka Metallov* **12** (1980) 19.
14. J. E. SMUGERESKY, *Met. Trans.* **8A** (1977) 1283.
15. L. S. DARKEN and R. P. SMITH, *Corrosion* **5** (1949) 1.
16. J. H. KEELER and H. M. DAVIS, *AIME Trans.* **197** (1953) 44.
17. M. L. HILL and E. W. JOHNSON, *Trans. TMS-AIME* **215** (1959) 717.
18. W. F. SAVAGE, E. F. NIPPES and E. I. HUSA, *Welding J.* **61** (1982) 233.
19. H. IKAWA, H. OSHIGE and S. NOI, *J. Welding (Jpn)* **7** (1977) 396.
20. D. ROSENTHAL, *Trans. ASME* **68** (1946) 849.

Received 28 January
and accepted 16 December 1987